IEEE Access
Multidisciplinary ⋮ Rapid Review ⋮ Open Access Journal

Received April 2, 2022, accepted April 18, 2022, date of publication April 22, 2022, date of current version April 28, 2022.

Digital Object Identifier 10.1109/ACCESS.2022.3169506

Design of Coaxial Integrated Macro–Micro Composite Actuator With Long-Stroke and High-Precision

CAOFENG YU, GAN WU, YU WANG, ZHIHAO XIAO, YONGYONG DUAN, AND ZHUO CHEN
School of Mechanical Engineering, Anhui University of Science and Technology, Huainan, Anhui 232001, China

Corresponding author: Caofeng Yu (yucaofeng@aust.edu.cn)

This work was supported in part by the National Natural Science Foundation of China under Grant 52105042, in part by the Anhui Provincial Natural Science Foundation under Grant 2008085QE214, and in part by the China Postdoctoral Science Foundation under Grant 2019M652159.

ABSTRACT Macro–micro composite-driving structures are widely used in many applications, and research has been done to improve the associated driving stroke and positioning accuracy. This article proposes a novel macro–micro composite actuator (MMCA) with a long-stroke and high-precision based on a voice coil motor (VCM) and giant magnetostrictive actuator (GMA). However, having a long stroke and high precision is contradictory. To verify this design scheme, the permanent magnet, coil, yoke, and other parts of the MMCA are designed and selected in detail. The axial and radial cross-sections of the macro-motion mechanism are studied using the magnetic equivalent circuit method. The force of the macro-motion coil is obtained based on finite element analysis (FEA). The results from both the FEA and practical experiments show the simulation results are consistent with the theoretical predictions. The maximum force of the MMCA is 53 N, the maximum displacement is 47 mm, the maximum positioning error is only 0.14μm, and the maximum acceleration is approximately 6.7g, which lays a theoretical and technical foundation to provide a high-performance actuator in the field of precision manufacturing.

INDEX TERMS Giant magnetostrictive actuator, voice coil motor, coaxial integration, long-stroke, high-precision.

I. INTRODUCTION

The equipment manufacturing industry is the basis for economic and social development. The actuator is a basic mechanical part that is the core power device of mechanical equipment [1], [2]. A giant magnetostrictive actuator (GMA) is an energy conversion device that converts electromagnetic energy into mechanical energy. These are developed based on the magnetostrictive effect of giant magnetostrictive materials (GMMs) to form a precise actuator that has the advantages of a high positioning accuracy, large output force, and strong stability. This has great potential application value in the field of precision manufacturing, but its maximum driving stroke can only reach the micron level, which significantly restricts the development of its engineering applications [3].

The associate editor coordinating the review of this manuscript and approving it for publication was Yingxiang Liu.

The stroke of the GMA increases with the magnetostriction coefficient and length of the GMM. However, considering the production level of GMMs and the size of the actuator itself, the stroke has a limited ability to increase due to bounds on the magnetostriction coefficient and length [4]. Therefore, this problem must be solved in other ways. The macro–micro combined drive method is another way to increase the stroke. This divides the drive system into two parts: macro- and micro-actuators. The macro-actuator realizes large-scale and high-speed coarse positioning, and the micro-actuator realizes small-scale, high-speed precision positioning.

Scholars have researched macro and micro composite actuator. For example, the United States Integrated Solution company [5] developed a precision positioning table for lithography machines. The macro motion table holds a 200-mm movement stroke through an air-floating guide rail, which finally gives a positioning accuracy of 20 nm for

the system. Kawashima et al [6] designed a macro–micro actuator device where the macro-moving component uses a pneumatic servo cylinder as the power source. The micro-movement components are driven using pneumatic bellows. Heui [7] used a DC servo motor to drive a ball screw in conjunction with a piezoelectric ceramic actuator to achieve a macro and micro two-level positioning system. Position feedback was achieved with an accuracy of 10 nm within a 200 mm movement stroke. Sakton et al [8] used a permanent magnet linear motor as a macro-motion actuator, and piezoelectric ceramics combined with a flexure hinge as a micro-motion drive to develop a combined macro–micro drive.

Compared with the traditional driving platform, the macro-micro motion platform has obvious advantages in positioning accuracy and response speed, Professor Deng Yongjun [9] and others developed a new type of linear worktable and proposed a two-dimensional compensation method for straightness error and positioning error based on macro-micro motion control. Its structure has been improved to reduce the straightness error on the horizontal plane and realize the straightness error of 0.55μm/100mm and the forward and reverse positioning errors of 0.69μm/100mm and 0.79μm/100mm. Professor Zhang Lufan [10] and others have developed a macro-micro composite actuator platform, which is composed of VCM and PSA. Based on the double axis parallel flexure hinge mechanism, the linear motion guidance and PSA preload are realized, which improves the accuracy of the system to the level of 20nm, overcomes the spear between high acceleration and nano accuracy, and greatly improves the performance of the system. Professor Zhang Lanyu [11] and others experimented with an adaptive damping method on the macro-micro workbench with large stroke, defined and determined the starting conditions and expansion principle of the damping element (pzt_2) used in this method. For the stroke of 40mm, the speed of 0.2m/s, the acceleration of 40 m/s^2 and the positioning accuracy of $\pm 3\mu$m motion, the stability time of macro-motion is shortened by 54.4%.

Zhu Yu *et al.* [12] developed a motion platform for a lithography machine that uses a permanent magnet linear motor to drive the macro stage and an air bearing and a VCM to drive the micro stage. The working stroke reached 300 mm and the positioning accuracy reached 12 nm. Wang Lisong [13] successfully developed an ultra-precision positioning table with a linear motor to develop a large displacement drive and an electrostrictive micro-displacer to achieve a precision drive. The working stroke was 500 mm and repeated positioning had an accuracy of 20 nm. Sun Baoyu *et al.* [14] developed an ultra-precision positioning table that used servo motors and ball screws for a large displacement drive and piezoelectric ceramics to achieve a precise displacement drive with a positioning accuracy of 10 nm. In addition, Professor Liu [15], Professor Ru [16], Professor Tian [17], Professor Zhang [18], and Professor Gao [19] designed different macro and micro composite platforms with different control methods, and achieved good control results.

In summary, existing macro–micro composite drive structures have two primary forms: stacking [20] and coaxial centering [21] types. The stacking type superimposes the micro-actuator on the macro-actuator. When the macro-actuator moves, the micro-actuator is driven so they move together. This installation has a simple structure and is easily realized. However, the macro/micro-actuator is not on the same axis, which causes Abbe errors to occur and leads to inaccurate displacement measurements that affect the control accuracy. The coaxial centering type places the macro- and micro-actuators on the two ends of the workbench and keeps their axes aligned. Although this installation can avoid Abbe errors during measurements, the axis of the macro/micro-actuator must be kept aligned during installation, which provides higher requirements for structural installations, and makes the overall structure of the workbench more complex.

In view of the above problems, according to the accumulation of previous research, this paper compares the structures of voice coil motor and giant magnetostrictive actuator. It is found that both voice coil motor and giant magnetostrictive actuator adopt electromagnetic drive, which can connect the shell of giant magnetostrictive actuator with the coil frame of voice coil motor, so that the giant magnetostrictive actuator moves with the moving parts of voice coil motor, To realize macro movement; At the same time, when the giant magnetostrictive actuator moves with the voice coil motor as a whole, micro-motion is realized by controlling the output displacement of the giant magnetostrictive actuator; By improving the existing structure, the two can always keep coaxial in structure, and integrate the macro-motion part and micro-motion part into one, so as to realize a high degree of coaxial integration.To overcome the shortcomings of existing macro–micro composite driving methods, this paper proposes a simple structure, convenient installation, and facile integration based on the Ampere force driving principle of the VCM and the magnetostrictive effect of the GMMs. The design scheme of the coaxial integrated MMCA gives a zero theoretical Abbe error. The permanent magnet, drive coil, and yoke structure of the macro-motion mechanism are designed in detail. The axial section and diameter of the macro-motion mechanism are simulated and analyzed. The performance of the coaxial integrated MMCA is tested through experiments, which verifies the feasibility of the proposed design scheme and lays a theoretical foundation to provide a high-performance actuator in the field of precision manufacturing.

II. STRUCTURE OF COAXIAL INTEGRATED MMCA

The detailed design scheme of coaxial integrated MMCA is given, including the structural design scheme of MMCA, the permanent magnet structure design of large motion mechanism, the drive coil design of micro motion structure and the yoke structure design and material selection of

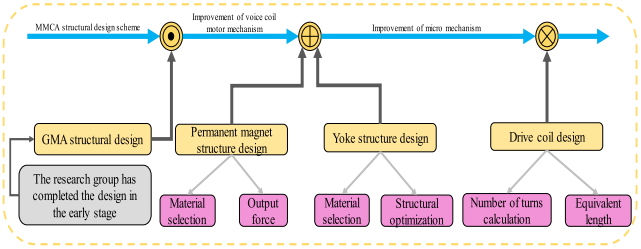

FIGURE 1. Structure of coaxial integrated MMCA.

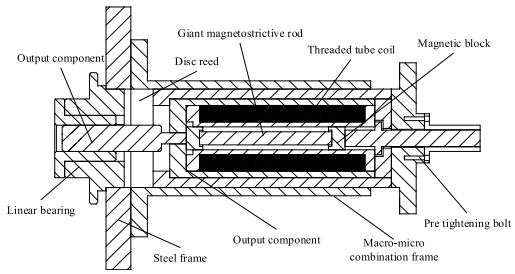

FIGURE 2. Structure diagram of main components of giant magnetostrictive actuator.

TABLE 1. Basic structural parameters of microactuator.

Names	Parameter values
GMM rod length (mm)	80
GMM diameter (mm)	8
Output rod diameter (mm)	12
Maximum outer diameter of micro actuator (mm)	60
Maximum length of micro actuator (mm)	132

large motion mechanism. The design flow chart is shown in FIGURE 1.

A. STRUCTURAL DESIGN SCHEME OF MMCA

The structural design of the micro-motion GMA was completed in early stages [3], Its main structure is shown in FIGURE 2. The basic structural parameters of the micro-motion part designed by the research group are shown in Table 1. The micro-motion structure of the giant magnetostrictive actuator uses the principle that the magnetostrictive functional material will expand axially in a changing magnetic field. When a controllable magnetic field is input, the giant magnetostrictive rod can be controlled to output a given displacement. the macro-motion structure of the MMCA is mainly designed here. As shown in FIGURE 3(a), the structure of a traditional VCM mainly includes a drive coil, a permanent magnet as the magnetic field source, a coil motion support frame, and a magnetic yoke for the magnetic circuit. To realize the macro–micro composite actuator structure, the structure of a traditional VCM is modified, as shown in FIGURE 3(b).

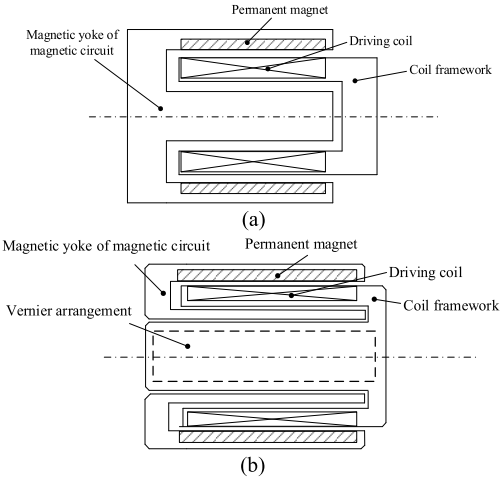

FIGURE 3. Structural scheme for the macro-motion mechanism. (a) Structure of traditional VCM. (b) Improved VCM structure.

TABLE 2. Properties of the 38H neodymium iron boron ($Nd_2Fe_{14}B$).

Parameters	Magnetic field intensity (T)	Energy (KJ/m^3)	Working temperature (°C)
Values	1.24–1.30	288–304	≤ 80

From FIGURE 3, the structure of the proposed coaxial integrated MMCA improves the structure of the traditional VCM and embeds the GMA coaxially inside it, which is consistent with the traditional superimposed macro–micro composite structure. In comparison, the proposed structural scheme has the advantages of high integration, large load capacity, fast response speed, and zero Abbe error in theoretical measurements.

B. PERMANENT MAGNET STRUCTURE DESIGN OF THE MACRO-MOTION MECHANISM

The 38H neodymium iron boron (Nd2Fe14B) permanent magnet material is selected as the magnetic field source for the macro-motion mechanism, and its material properties are given in Table 2.

The working principle of the VCM is based on Ampere's force law. When the magnetic field strength is perpendicular to the current flow, the expression for the output force is shown as:

$$F_P = B_g L_q I \tag{1}$$

where: Bg is the magnetic field strength generated by the permanent magnet at the air gap of the drive coil, units: T; Lq is the extended length of the drive coil, units: m; and I is the current flowing through the drive coil, units: A.

Equation (1) indicates that the output force Fp of the macro-motion mechanism is affected by three factors: Bg, Lq, and I. To simplify the control of the subsequent output force Fp, the design of the drive magnetic field should be as close as possible to the magnetic field at the air gap of the drive

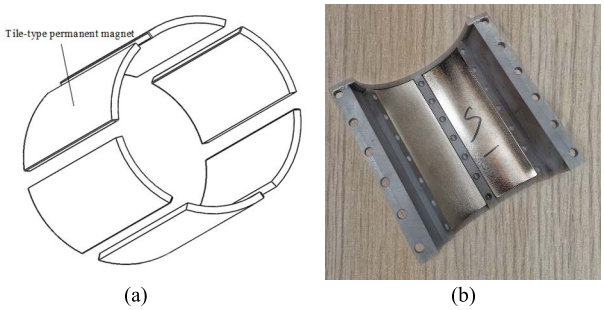

FIGURE 4. Magnetic field source permanent magnet array for the macro-motion mechanism. (a) Schematic diagram. (b) Photograph.

coil. The strength is uniform, and the ideal magnetic field source permanent magnet structure should be a ring structure. However, the ring structure of the $Nd_2Fe_{14}B$ is more difficult for processing and radial magnetization. To reduce difficulty in the permanent magnet design and manufacturing, this paper adopts an a ring-shaped array of six-piece permanent magnets to replace the single ring-shaped permanent magnet. Its structure is shown in FIGURE 4.

C. DESIGN OF DRIVING COIL FOR MACRO-MOTION MECHANISM

FIGURE 5 is the structure of the macro–micro connecting frame with a driving coil for the macro-motion mechanism. The driving coil is the actuator that pushes the macro–micro connecting frame and micro-motion part. The received driving force comes from the coil current in the air gap magnetic field. Therefore, the parameters that affect the Ampere force that is received by the coil are the air gap magnetic flux density Bg, the equivalent coil length Lq, and the coil current I. The air gap flux density Bg depends on the maximum energy product of the permanent magnet and the shape of the magnetic circuit for the magnetic yoke. The coil current I depends on the output from the current source.

The driving coil is usually a spiral wound with enameled wire. As seen from FIGURE 5, the number of driving coil turns depends on the length Lc and thickness dc of the macro-moving bobbin coil slot, the total number n of driving coils as:

$$n = \frac{L_c}{D_q} \cdot \frac{d_c}{D_q} \tag{2}$$

where: Dq is the diameter of the enameled wire; The number of turns n provides the total equivalent length Lq of the coil, which is given as:

$$L_q = \pi n \frac{d_{max} + d_{min}}{2} \tag{3}$$

where: dmax is the center diameter of the outer ring of the coil group, units: m; and dmin is the center diameter of the innermost ring of the coil group, units: m.

$$d_{min} = d_h + D_q + 0.05 \tag{4}$$

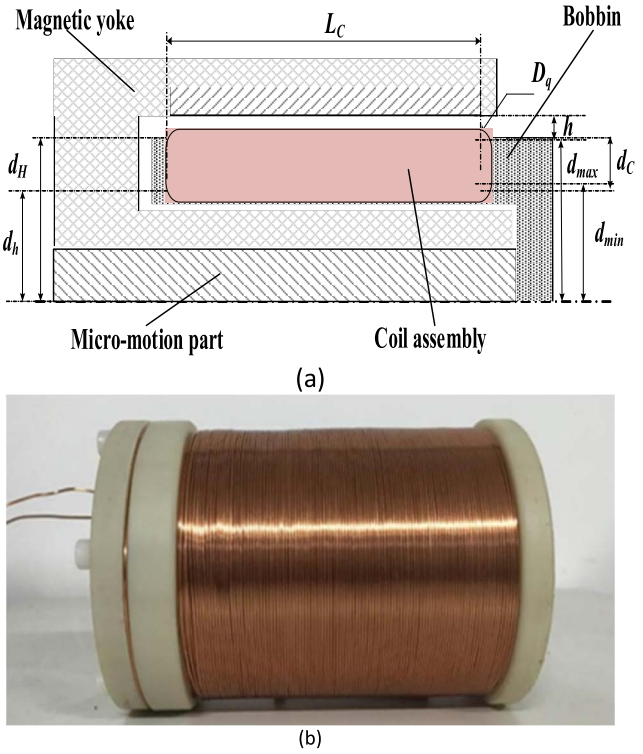

FIGURE 5. The structure of the macro–micro connection frame and the drive coil. (a) Schematic diagram. (b) Photograph.

where d_h is the diameter of the bottom end of the coil slot and 0.05 is the thickness of the enameled wire. The center diameter Dmax of the outermost ring of the coil group of the macro micro connection frame is:

$$d_{max} = d_h + 2n_2 \cdot D_q + 0.05 \times 2n_2 \tag{5}$$

In an ideal state, Where $d_n = 76$mm, if an enameled wire with a diameter of 1 mm is used, the number of coils on the macro–micro connector with a thickness can reach dc. However, to prevent rubbing, this gives windings of 110 mm with a thickness for the bobbin of 8 mm. The actual number n of windings is 632 and the total length Lq is 163.9 m.

D. YOKE STRUCTURE DESIGN AND MATERIAL SELECTION FOR THE MACRO-MOTION MECHANISM

The role of permanent magnets in the magnetic circuit is similar to the voltage source in the circuit, and the magnetic flux is similar to the current. If it is assumed that a working air gap is an electrical appliance, the yoke can be compared to a wire, which plays a role in the magnetic circuit. To determine the magnetic flux, the yoke should be made of the material with the strongest magnetic permeability in the magnetic circuit, which is generally a soft-iron material. Common soft iron materials include nickel-iron alloys, pure iron, silicon steel sheets, and certain iron alloys. Compared with other materials, such as aluminum, copper, ordinary steel, and other non-ferrous alloys, soft-iron materials have greater relative magnetic permeability and smaller residual magnetic flux Br and coercive force Hc.

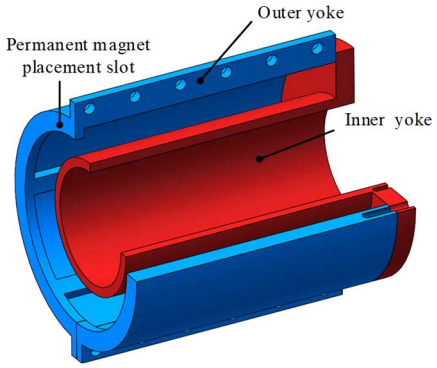

FIGURE 6. Atic diagram for the structure of the macro moving yoke.

The structure of the proposed macro-moving yoke based on the rationality of the macro–micro composite drive embedded structure and magnetic circuit distribution is shown in FIGURE 6. The macro-moving yoke not only utilizes the macro-moving permanent magnet to produce a constant magnetic field in the working air gap, but the condition of the air gap flux is also reasonable in terms of space for the micro-movement part and the overall construction and assembly. In FIGURE 6, there are six permanent magnet placement slots in the outer magnetic yoke of the macro movement. The inner yoke is the working air gap that meets the movement space of the coil frame. The yoke returns to the S pole of the permanent magnet through the working air gap.

III. OVERALL STRUCTURE SCHEME AND WORKING PRINCIPLE OF COAXIAL INTEGRATED MMCA

A. OVERALL STRUCTURE OF MMCA

As shown in FIGURE 7. the proposed coaxial integrated MMCA structure mainly includes a rear ejector shaft, rear sliding bearing, rear cover, macro-moving inner yoke, macro-moving outer yoke, tile-type permanent magnet, macro-movement coil, macro-movement coil former, magnetic isolation cylinder, micro-movement yoke sleeve, micro-movement coil, micro-movement coil former, GMM rod, magnetic block, magnetic ring, disk spring, micro-movement yoke, macro–micro connecting frame, outer bracket, output sleeve, front sliding bearing, and output rod. The six-piece permanent magnets are fixed on the inner wall of the shell. The macro-moving coil bobbin is placed inside the tile-shaped permanent magnet, and the macro-moving coil bobbin is outside the macro-motion coil and connected around. The micro-motion coil skeleton is arranged inside the macro-motion coil skeleton, the micro-motion coil skeleton is surrounded by the micro-movement coils, and the GMM rod is placed on the micro-motion coil skeleton. Both ends of the GMM rod are provided with magnetic conductive blocks to increase the magnetic field strength at the axis position. A cooling water pipe is wound around the periphery of the GMM rod for heat dissipation to increase its performance.

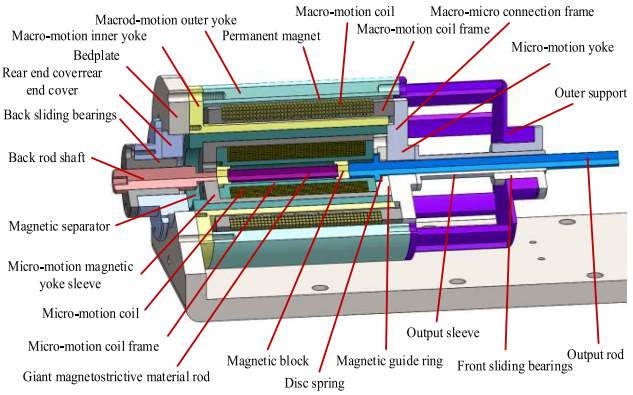

FIGURE 7. Three-dimensional schematic diagram of the MMCA.

TABLE 3. Weight and working air gap parameters of macro-micro actuator.

Names	Parameter values
Total mass of mover (kg)	4
Maximum outside diameter of micro actuator （mm）	60
Maximum length of micro actuator (mm)	132
Number of drive coil windings	632
Total length of drive coil （m）	163.9
Total mass of working platform(kg)	1.3
Air gap size of voice coil motor(mm)	1.9
Motion friction （N）	7

The space where the drive coil moves in the voice coil motor is called the working air gap. The gap width of the working air gap will affect the magnetic field strength of the air gap. When the voice coil motor works, its magnetic circuit must remain closed. The magnetic conduction circuit is similar to the conductor of the circuit, and the working air gap is similar to the resistance. If the air gap is too large, the magnetic flux of this circuit will be reduced. Therefore, the working gap of the air gap of the magnetic circuit should be set at an appropriate value. The quality will affect the start, acceleration and stop of the motor, and then affect its control accuracy by affecting its reflection speed,The specific parameters are shown in Table 3.

B. WORKING PRINCIPLE OF THE MMCA

The working process of the coaxial integrated MMCA is divided into two parts: macro- and micro-motion. The macro-motion principle is equivalent to the VCM, and the micro-motion part is equivalent to the GMA. A schematic diagram of the associated working principle is shown in FIGURE 8.

The working process of the proposed MMCA is divided into three stages: the initial zero stage, the macro-motion positioning stage, and the micro-motion compensation stage, as shown in FIGURE 9. and FIGURE 10.

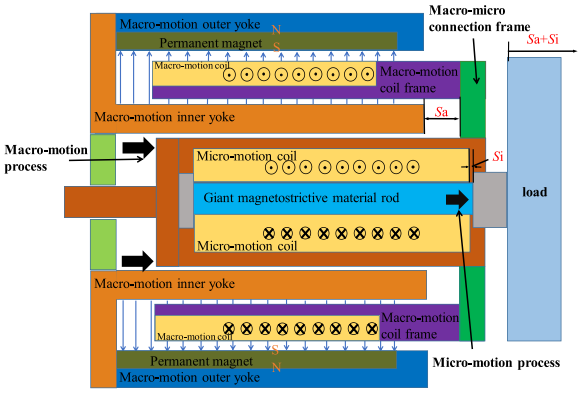

FIGURE 8. Schematic diagram for the working principle of the MMCA.

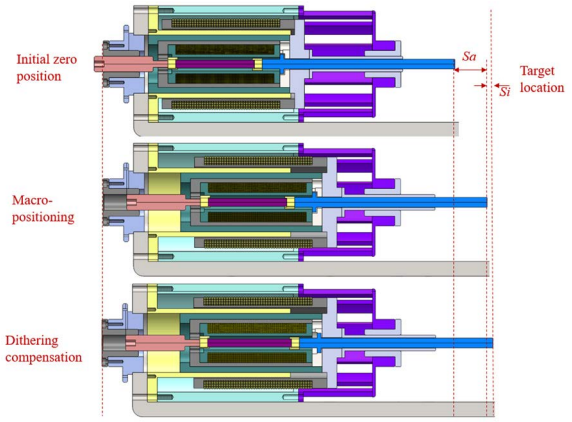

FIGURE 9. Working process of the MMCA.

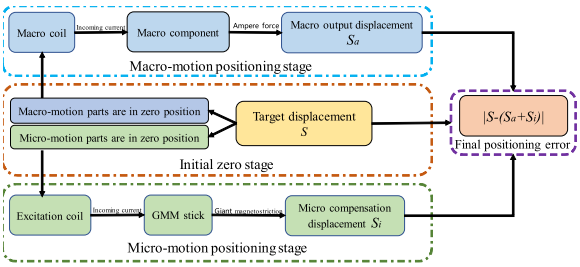

FIGURE 10. MMCA control flow chart.

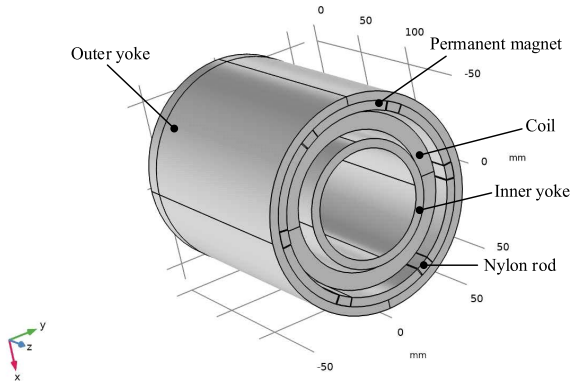

FIGURE 11. Three-dimensional diagram of the macro-motion structure of the MMCA.

1) Initial zero-position stage. At this stage, the MMCA is in the zero-position state. The macro- and micro-moving components are both in the zero position.

2) Macro-movement positioning stage. When the macro-moving coil is supplied with a current Ima, Ampere's law indicates that the macro-moving coil is affected by the Ampere force F. Under the action of the Ampere force F, this overcomes the frictional force f, the macro-motion coil, the macro-motion, the coil bobbin, and all its internal components move together along the drive axis to realize macro-motion positioning. The acceleration, speed, and distance of the macro-motion components can be controlled by adjusting the size and time of the macro-motion coil current Ima.

3) Micro-motion compensation stage. The function of the micro-motion stage is to compensate for the macro-motion positioning process. Its operational principle is that when the macro-motion positioning distance Sa deviates from the ideal positioning distance Si, a current Imi is passed through the micro-motion coil so that the moving coil forms an energized solenoid, which generates an internal axial magnetic field H. Due to the magnetostrictive effects of the GMM rod, the magnetic field strength H causes the GMM rod to deform and extend, which pushes the output rod and compresses the disc spring. This displaces the output rod and realizes micro-movements. Adjusting the micro-movement coil current Imi controls the size of the generated magnetic field H, which then adjusts the elongation of the GMM rod to control the micro-movement displacement value close to Si and compensates for the macro-motion positioning error. Comprehensively adjusting the macro-moving coil current Ima and the micro-moving coil current Imi allows ultra-precise positioning of the MMCA within a long stroke range.

IV. SIMULATION OF THE COAXIAL INTEGRATED MMCA

A. SIMULATION OF THE AXIAL SECTION OF THE MACRO-MOTION MECHANISM

The overall three-dimensional structure of the MMCA can be obtained from the permanent magnet, coil, and yoke design, and the simulation model is established in the geometry module within COMSOL, as shown in FIGURE 11. The material properties related to the magnetic field analysis of each structure of the macro-motion mechanism selected from the built-in material library in COMSOL are shown in Table 3.

The current of the drive coil is set to 0 A to explore the distribution law of the magnetic flux for the six-piece permanent magnet in the macro-motion mechanism. The associated magnetic field distribution of the macro-motion mechanism is shown in FIGURE 12. The magnetic flux density modulus has units of T. The magnetic flux flow direction arrow distribution rule for the permanent magnet

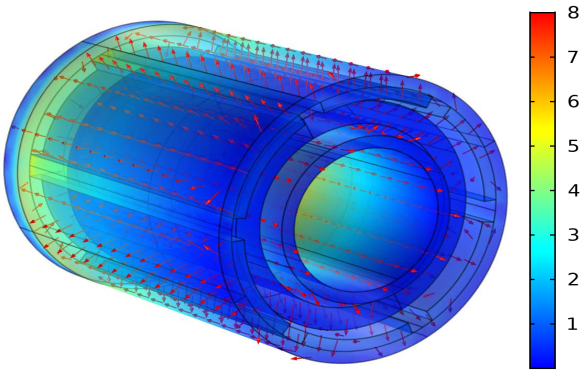

FIGURE 12. Magnetic flux density distribution diagram of the permanent magnet for the macro-motion mechanism.

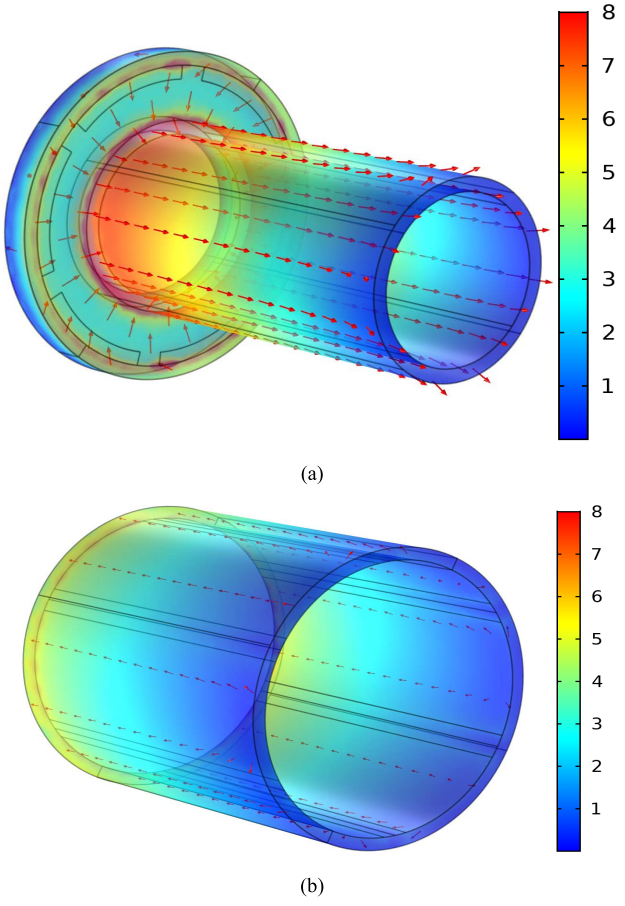

FIGURE 13. Distribution diagram of the magnetic flux density mode of the inner and outer yokes. (a) the outer yoke. (b) the inner yoke.

of the macro-motion mechanism is that the outer yoke is from front to back, the inner yoke is from back to front, and the air-gap flux at the coil is radially from the inside to outside. This is similar to the theoretically derived magnetic flux distribution law in the axial section reluctance equation.

It is seen from FIGURE 12 and FIGURE 13 that the average magnetic flux density modulus at the front end of the inner and outer yokes is smaller than the average flux

TABLE 4. Related parameters for macro-motion magnetic field analysis.

Structure name	Material	Relative permeability	Others
Outer yoke	Soft iron	2180	B-H curve
Inner yoke	Soft iron	2180	B-H curve
Coil	Copper	1	632 turn 0~4A
Coil skeleton	Nylon	1	
Air gap	Air	1	
Permanent magnet	N38NdFeB	1	Remanence 1.21T

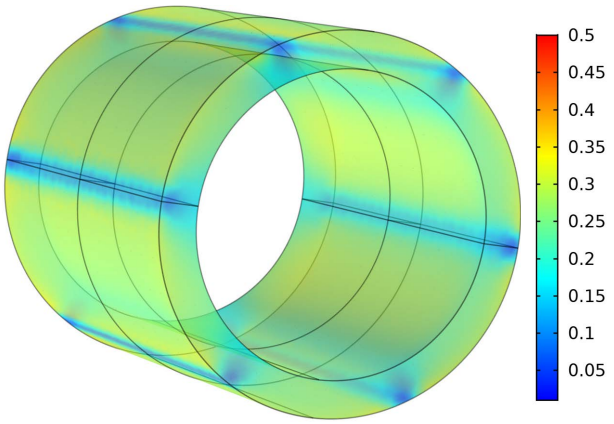

FIGURE 14. Air gap magnetic flux density distribution at the driving coil.

density modulus at the rear end. Thus, the magnetic flux density distribution at the yoke in the closed magnetic circuit of the macro-motion mechanism is unequal, which shows an increase from front to back. The inner magnetic yoke flows from back to front, and the outer magnetic yoke flows from front to back.

Although the magnetic flux density distribution of the yoke is non-uniform, the Ampere force experienced by the coil is affected primarily by the air gap magnetic flux density mode at the coil. Therefore, this does not directly impact the Ampere force received by the driving coil. The air-gap flux density distribution at the driving coil is shown in FIGURE 14. The air gap magnetic flux distribution at the drive coil is relatively uniform overall, and the arrows representing the magnetic flux flow direction are radially distributed from inside to outside. This is consistent with the analysis results from the axial section magnetic circuit equation for the macro-motion mechanism. FIGURE 14 illustrates that there are six low-value magnetic flux areas in the air gap magnetic flux distribution of the driving coil. Compared with the three-dimensional model, these magnetic flux areas are all located at the junction of the six-piece permanent magnet.

As the three-dimensional structural simulations give too much attention to the overall magnetic flux density distribution, it is difficult to observe and analyze the uneven magnetic flux density distribution at the air gap as caused by the non-integral ring structure of the six-piece permanent magnet.

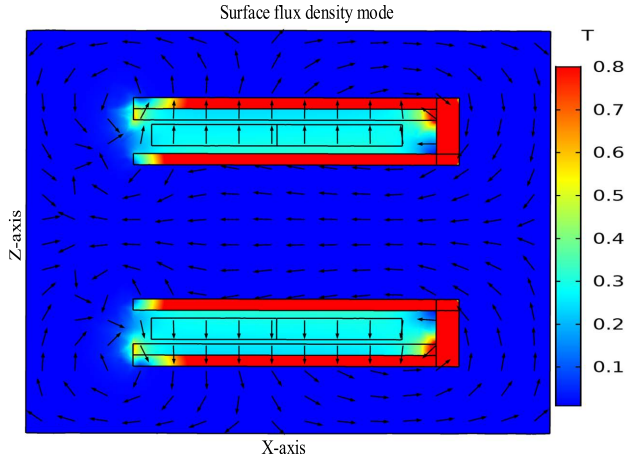

FIGURE 15. Magnetic flux density distribution in the middle section of the permanent magnet.

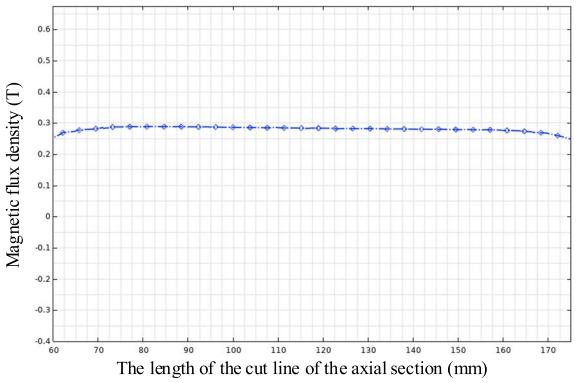

FIGURE 16. Magnetic flux density modulus curve for the air gap in the middle section of the permanent magnet.

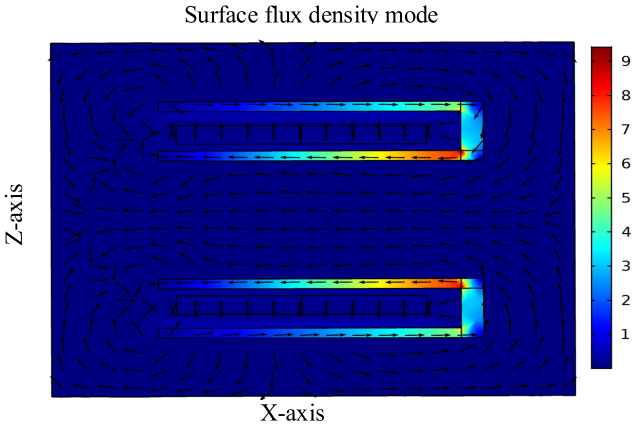

FIGURE 17. Axial sectional magnetic field flux density distribution at the junction of permanent magnets.

Therefore, it is necessary to analyze the macro-motion mechanism of the cross-sectional magnetic field distribution state in some areas.

First, the axial section is taken from the middle of the monolithic permanent magnet in the three-dimensional model, and the magnetic flux density distribution of the magnetic field after the axial section is obtained, as shown in FIGURE 15. The magnetic flux at the air gap of the monolithic permanent magnet flows in the direction of the arrows from the inside to the outside in the radial direction. Except for the uneven distribution of the magnetic flux density at the front and bottom of the working air gap, the central magnetic flux density distribution for the region is relatively uniform. The uniform region accounts for more than 90% of the total air gap cross-sectional area.

A cut line is selected in the interface to further obtain the specific magnetic flux density at the working air gap. The length of the cut line for the axial section is 115 mm. The starting point is 5 mm from the back end of the coil, and the ending point is at the front end to provide an air gap curve for the magnetic flux density mode is shown in FIGURE 16. The uniformity of the air gap magnetic flux density distribution in the axial section as taken from the middle of the monolithic permanent magnet is relatively uniform and about 0.3 T.

The axial section in the middle of the junction for the permanent magnet is intercepted based on the three-dimensional model. The magnetic flux density distribution after the axial section is obtained is shown in FIGURE 17. There are two opposite directions for the air gap magnetic flux flow at the junction of the tile-shaped permanent magnet. The direction of the magnetic flux arrow from the inside to the outside in the radial direction is the air gap is generated from the axial section magnetic circuit of the macro-motion mechanism. The flow direction of the magnetic flux and the direction of the magnetic flux arrows from the outside to the inside in the radial direction represent the flow direction of the air gap magnetic flux at the junction of the permanent magnets in the radial section magnetic circuit of the macro-motion mechanism.

The parameters of the section line in the cross-section are the same as previous ones, and the associated air gap magnetic flux density distribution curve is shown in FIGURE 18. The air gap magnetic flux density distribution at the junction of the two tile-shaped permanent magnets is uneven, and the overall air gap magnetic flux average is significantly smaller than the average over the cross-section at the center of the permanent magnet and about 0.15 T.

B. SIMULATION OF THE RADIAL SECTION OF THE MACRO-MOTION MECHANISM

The cross-sectional magnetic flux density distribution of the radial section is shown in FIGURE 19. The air gap magnetic flux density at the driving coil has a low area at the junction of the 6-W permanent magnets (black area in the figure), and the air gap magnetic flux flow direction arrows in the six low-value areas have opposite arrows. This result is the same as that for the axial cross-sectional magnetic field distribution at the junction of the permanent magnet described above. To obtain a specific value for the air gap magnetic flux density, a circular ring on the radial section is intercepted,

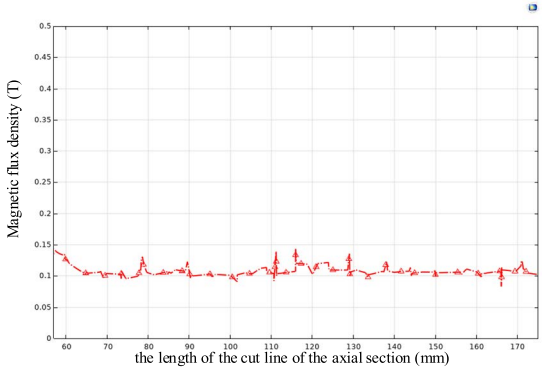

FIGURE 18. Magnetic flux density modulus curve on the section line at the junction of permanent magnets.

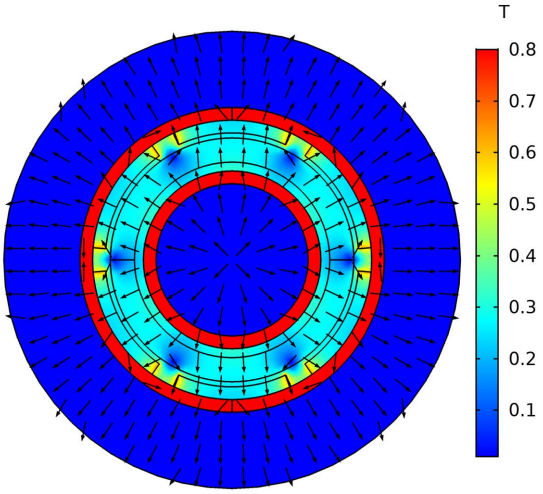

FIGURE 19. Magnetic flux density distribution after radial section.

which is located inside the coil. The magnetic flux density distribution approximately represents the overall distribution law of the air gap magnetic flux density at the coil.

The obtained magnetic flux density mode distribution curve on the toroidal section is shown in FIGURE 20. The air gap magnetic flux density mode at the drive coil has a significant low-value area (low valley), but there is a high-value area (peak) at both ends. The flux distribution is non-uniform, but after the high- and low-value areas are superimposed, the overall magnetic flux density mode in the high-value area compensates for the partial magnetic flux density mode in the low-value area. Thus, the uniformity is improved. To further explore the influence of the unevenness on the Ampere force received by the driving coil, the force of the driving coil for the macro motion mechanism is simulated below.

C. FORCE SIMULATION OF THE DRIVING COIL FOR THE MACRO-MOTION MECHANISM

The maximum displacement of the drive coil is set to 40 mm and the maximum current is 4 A. The distribution of the magnetic flux density mode of the macro-motion mechanism

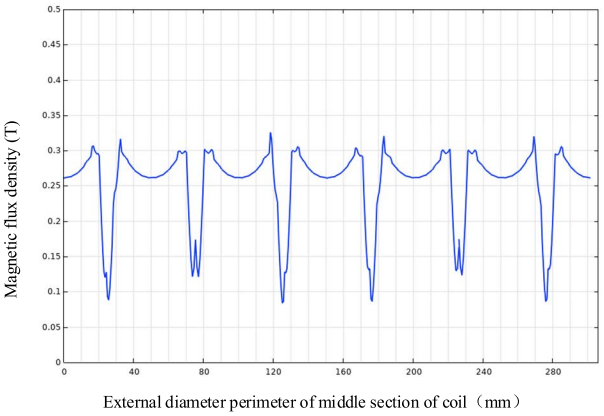

FIGURE 20. Magnetic flux density mode distribution curve on the toroidal section.

at different displacements is obtained via simulations. The magnetic flux distribution cloud diagrams at displacements of 0, 20, and 40 mm are shown in Figs. 21(a), 21(b), and 21(c). Changes in the magnetic flux received by the driving coil during the movement process obtained in the simulations are consistent with the theoretical analysis.

The force calculation module is used to determine the force F of the driving coil with the displacement S and the current I through further simulations, as shown in FIGURE 22. The force F of the drive coil increases with the current I and decreases with the displacement S. However, as the displacement S increases, the force F and linearity decrease. This is because the increased displacement S causes the coil to stretch. Outside of the permanent magnet, the length of the conductor that generates the Ampere force is reduced, and the force F and linearity both decrease.

V. EXPERIMENTAL VALIDATION

A prototype of the coaxial integrated MMCA is produced to further verify the feasibility of the proposed design scheme. An experimental test platform is built to determine the maximum motion stroke of the macro-moving component. The parameters for the maximum force and the minimum positioning error and maximum acceleration are measured.

The schematic diagram of the controller is shown in Figure 23. The control system equipment adopts voice coil motor driver (PAC483A), and the network control adopts Modbus RTU protocol. The default "communication rate" of the system is 115200bps, and the experimental voltage is 48V. In the closed-loop debugging process of the controller, in order to achieve the best effect, the S-type acceleration and deceleration curve is used for closed-loop parameter debugging, and then the better K_p and K_d are determined according to the K_i parameter value of PID empirical adjustment method. At the same time of PID operation, it is also necessary to calculate the feedforward compensation process. Proper K_{vff} can improve the dynamic tracking performance, make the actuator motion softer and the noise less. K_c can suppress the jitter or roar of the actuator in

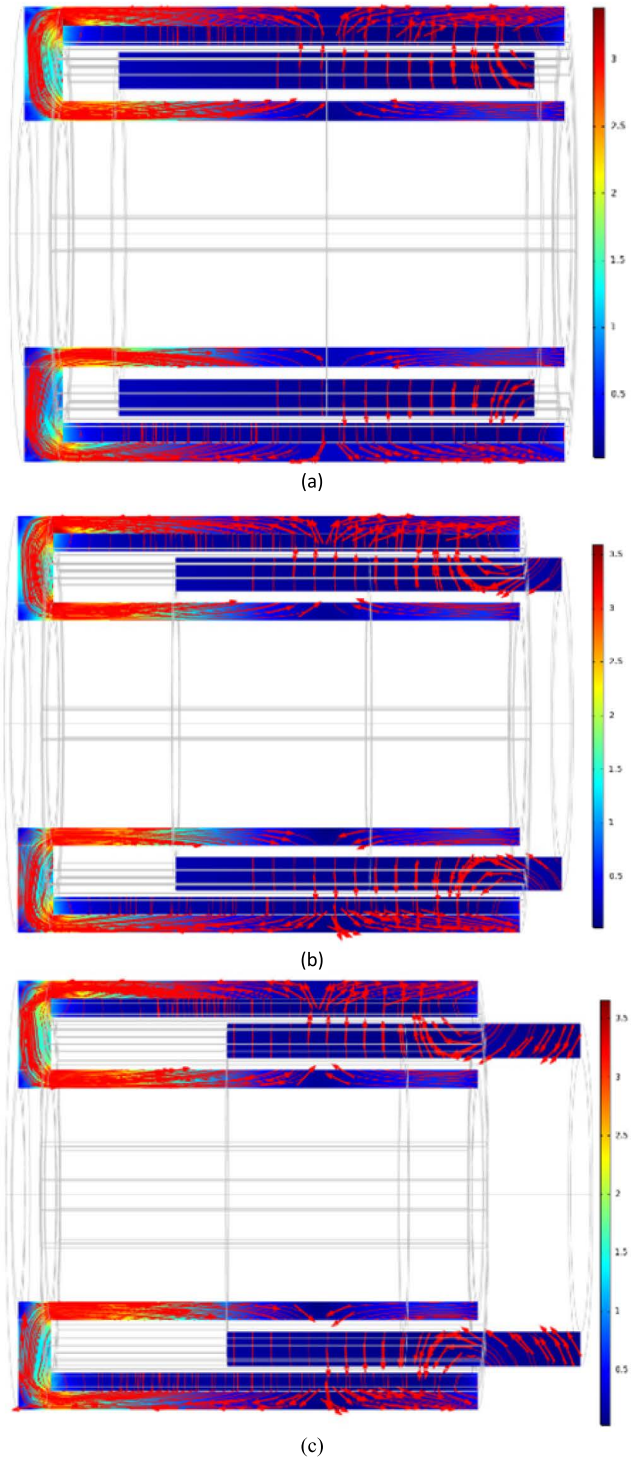

FIGURE 21. Distribution cloud map of the magnetic flux density mode at different displacements. (a) S = 0 mm. (b) S = 20 mm (c). S = 40 mm.

the steady state. After accumulating the feedforward and feedback adjustment formulas, the macro-motion part can achieve the best ability to eliminate the positioning error.

A. MAXIMUM FORCE TEST

The experimental platform to test the maximum force is shown in FIGURE 24, which is composed primarily of

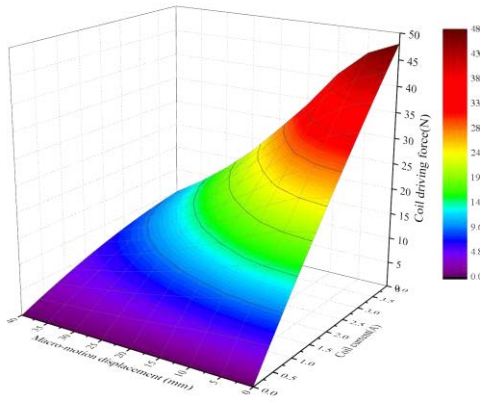

FIGURE 22. Force curve of the drive coil at different displacements and currents.

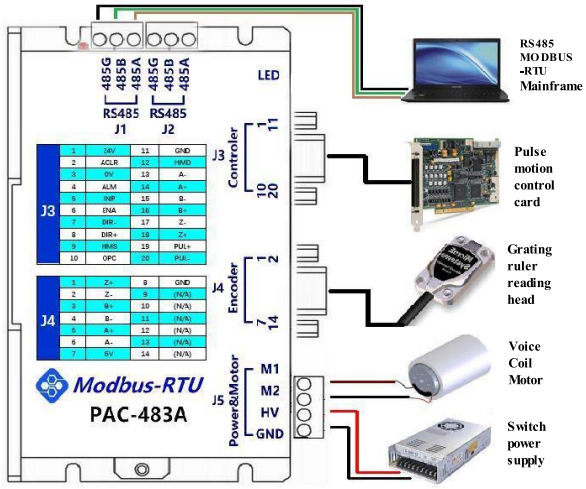

FIGURE 23. Schematic diagram of controller.

the MMCA, working platform, grating probe, force sensor, voltage source, switching power supply, and computer. The thrust curve of the MMCA after the experimental test is shown in FIGURE 25. When the macro-coil current of the MMCA is 4.5 A, the thrust reaches 53 N, and the test thrust is close to the simulations. the analysis of FIGURE 25. shows that the thrust value and simulation value fluctuate under the action of different currents. The main reason is that there are processing and assembly errors of parts, resulting in a certain coaxiality error of the assembled macro-micro composite actuator, so that the friction to be overcome is different at different positions and different experimental conditions.

B. MAXIMUM MOVEMENT STROKE AND MAXIMUM POSITIONING ERROR TEST

The experimental platform built to test the maximum movement stroke and maximum positioning error is shown in FIGURE 26. The platform is composed primarily of a coaxial integrated MMCA, a workbench, a grating probe, a switching power supply, a controller, and a computer. The displacement

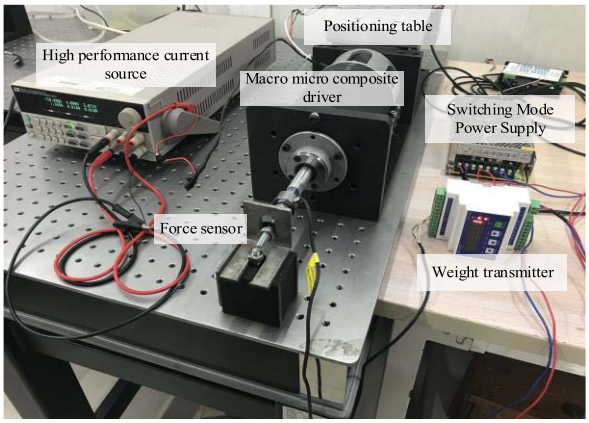

FIGURE 24. The maximum thrust test platform of the MMCA.

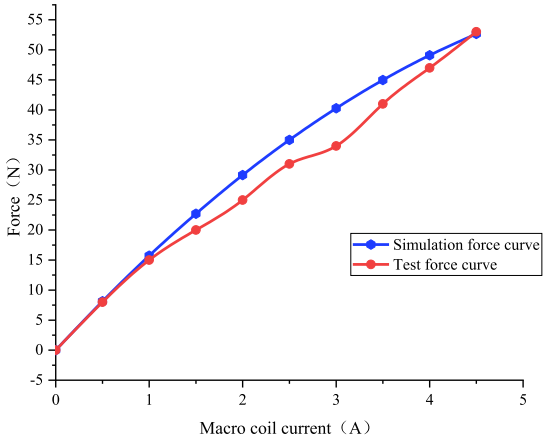

FIGURE 25. Thrust curves of the MMCA.

FIGURE 26. Experimental test platform for the maximum stroke and minimum positioning error.

curve and positioning error curve of the actuator are shown in FIGURE 27 and FIGURE 28 after experimental testing, Add 5N interference force to the macro part to obtain the load disturbance response curve of the macro part, as shown in FIGURE 29.

From FIGURE 27, the maximum stroke of MMCA reaches 47 mm, while the maximum driving stroke of the micro-motion part is only 37 μm. From FIGURE 28, the positioning error of the macro-motion part reaches 5 μm and

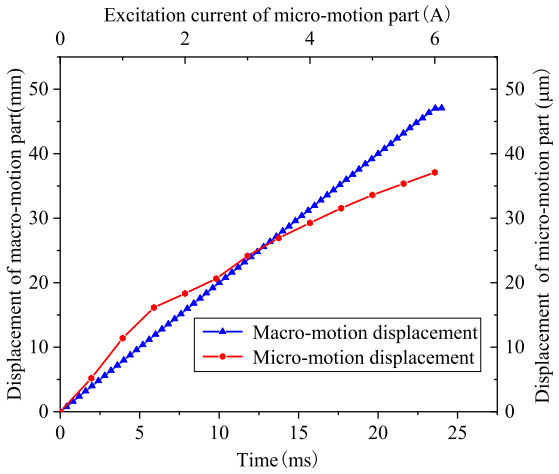

FIGURE 27. Displacement running curve of the MMCA.

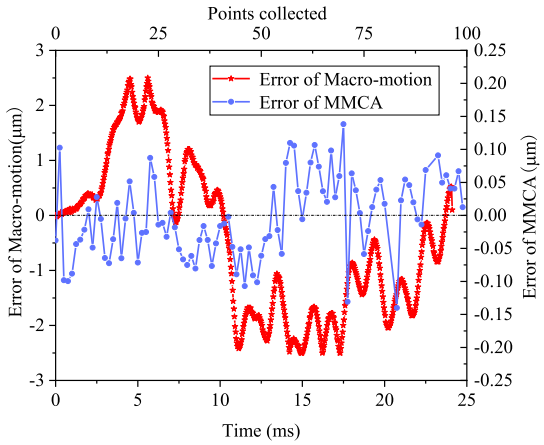

FIGURE 28. Positioning error curve of the MMCA.

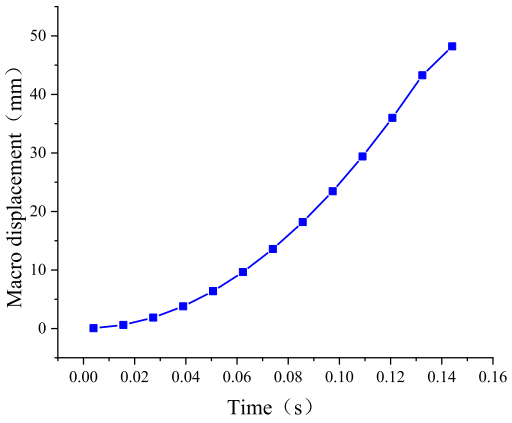

FIGURE 29. Response curve of load force to macro displacement disturbance.

the positioning error of the prototype is only 0.14 μm. It can be seen from FIGURE 29 that the influence of interference force on macro displacement gradually fades with the increase of operation time.the analysis of FIGURE 27 and FIGURE 28 and FIGURE 29 shows that the coaxial integrated MMCA has both the large stroke characteristics

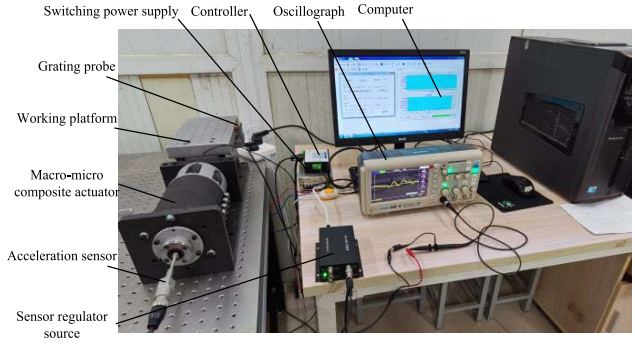

FIGURE 30. Test platform for the maximum acceleration.

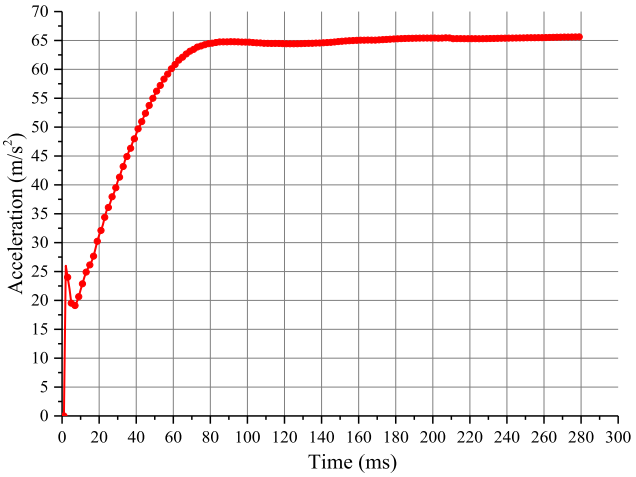

FIGURE 31. Acceleration operating curve for the MMCA.

of voice coil motor and the high-precision characteristics of *GMA*, which further demonstrates the feasibility of the design scheme

C. MAXIMUM ACCELERATION TEST

The experimental platform to test the maximum acceleration is shown in FIGURE 30, which is composed primarily of the MMCA, workbench, grating probe, sensor voltage stabilizer source, acceleration sensor, switching power supply, controller, oscilloscope, and computer. The acceleration running curve measured in the experiment is shown in FIGURE 31. According to the analysis FIGURE 31, the reaction time of sudden change of acceleration when the actuator is started is about 10ms The macro-motion maximum acceleration of the MMCA reaches 65.5 m/s^2, which is approximately 6.7 g with a final response time of about 80 ms.

VI. CONCLUSION

This paper combines the long-stroke characteristics of a VCM with the high-precision characteristics of the GMA and proposes a design scheme for a coaxial integrated MMCA. To verify the feasibility of the design, the macro-motion mechanism of the magnetic circuit is verified using the finite element method and experiments. The simulation results are consistent with the theoretical predictions. The experimental test results show that the maximum force of the MMCA is 53 N, and the maximum stroke is 47 mm. The maximum positioning error is only 0.14 μm, and the maximum acceleration can reach 6.7 g, with a response time of about 10 ms. This research results show that the design scheme of the proposed coaxial integrated MMCA is feasible and lays a theoretical and technical foundation for follow-up development of high-performance precision machining equipment.

REFERENCES

[1] Y. Cao and J. Dong, "Self-sensing and control of soft electrothermal actuator," *IEEE/ASME Trans. Mechatronics*, vol. 26, no. 2, pp. 854–863, Apr. 2021.
[2] B. Erkal, "On the performance of a fuzzy variable structure satellite attitude controller under sensor and actuator uncertainties," *Int. J. Signal Imag. Syst. Eng.*, vol. 12, nos. 1–2, Mar. 2021, Art. no. 113542.
[3] C. Yu, C. Wang, T. Xie, L. Yang, and Z. Jiang, "Development of drive system of high performance micro positioning worktable based on giant magnetostrictive material," *J. Mech. Eng.*, vol. 55, no. 9, pp. 136–143, May 2019.
[4] C. Yu, C. Wang, H. Deng, T. He, and C. Zhong, "Characteristics of magnetic domain deflection of $Tb_{0.3}Dy_{0.7}Fe_2$ alloy," *J. Rare Earths*, vol. 34, no. 9, pp. 882–888, Sep. 2016.
[5] T. Weichelt, Y. Bourgin, and U. D. Zeitner, "Mask aligner lithography using laser illumination for versatile pattern generation," *Opt. Exp.*, vol. 25, no. 18, pp. 20983–20992, Aug. 2017.
[6] K. Kawashima, "Robot surgical system using pneumatic actuators," *Int. J. Urol.*, vol. 25, p. 103, Oct. 2018.
[7] S. Barth, H. Bartzsch, D. Glöß, P. Frach, T. Modes, O. Zywitzki, G. Suchaneck, and G. Gerlach, "Magnetron sputtering of piezoelectric AlN and AlScN thin films and their use in energy harvesting applications," *Microsyst. Technol.*, vol. 22, no. 7, pp. 1613–1617, Jan. 2016.
[8] A. T. Salton, Z. Chen, J. Zheng, and M. Fu, "Constrained optimal preview control of dual-stage actuators," *IEEE/ASME Trans. Mechatronics*, vol. 21, no. 2, pp. 1179–1184, Apr. 2016.
[9] Y. Deng, X. Jin, and Z. Zhang, "A macro–micro compensation method for straightness motion error and positioning error of an improved linear stage," *Int. J. Adv. Manuf. Technol.*, vol. 80, nos. 9–12, pp. 1799–1806, Apr. 2015.
[10] L. Zhang, Z. Long, J. Cai, and J. Fang, "Design of a linear macro–micro actuation stage considering vibration isolation," *Adv. Mech. Eng.*, vol. 7, no. 5, May 2015, Art. no. 168781401558454.
[11] L. Zhang, J. Gao, X. Chen, Y. Chen, Y. He, Y. Zhang, H. Tang, and Z. Yang, "Implementation and experiment of an active vibration reduction strategy for macro-micro positioning system," *Precis. Eng.*, vol. 51, pp. 319–330, Jan. 2018.
[12] S. Lu, K. Yang, Y. Zhu, L. Wang, M. Zhang, and J. Yang, "Design and control of ultra-precision fine positioning stage for scanning bean interference lithography," *Acta Optica Sinica*, vol. 37, no. 10, pp. 202–210, Jun. 2017.
[13] L. Wang, B. Su, and S. Dong, "The research of high precision control methods for piezoceramic actuators," *Chin. Mech. Eng.*, vol. 13, no. 3, pp. 201–203, Feb. 2002.
[14] B. Sun, "Research on dynamic characteristic of micro-displacement mechanism based on piezoelectric actuator," *Piezoelectr. Acoustoopt.*, vol. 29, no. 6, pp. 653–655, Dec. 2007.
[15] H. Liu, "Research on macro/micro precision positioning and motion platform based on piezoelectric actuator," Jilin Univ., Changchun, China, Tech. Rep. 10183, Jun. 2016, pp. 5–6.
[16] Y. Wang, F. Sun, J. Zhu, M. Pang, C. Ru, and S. Campopiano, "Long-stroke nanopositioning stage driven by piezoelectric motor," *J. Sensors*, vol. 2014, no. 14, Nov. 2014, Art. no. 926314.
[17] Y. Tian, T. Wang, and M. Wang, "Compounding control of ultra-precision positioning stage based on inverse generalized PI model," *Chin. J. Mech. Eng.*, vol. 51, no. 2, pp. 198–206, Jan. 2015.

[18] T. Zhang, S. Li, L. Liang, Y. Liao, F. Cao, and S. Wen, "Design and analysis of a macro-micro linear piezoelectric motor micro driven mechanism," *J. Vib., Meas. Diagnosis*, vol. 37, no. 4, pp. 692–697, 838-839, Aug. 2017.
[19] L. Zhang, J. Gao, and X. Chen, "A rapid dynamic positioning method for settling time reduction through a Macro–Micro composite stage with high positioning accuracy," *IEEE Trans. Ind. Electron.*, vol. 65, no. 6, pp. 4849–4860, Jun. 2018.
[20] X. Chen, Y. Jiang, Y. Tan, J. Gao, Z. Yang, and G. Liu, "Progress and application of key technologies on the electronic packaging equipment development," *Chin. J. Mech. Eng.*, vol. 53, no. 5, pp. 181–189, Mar. 2017.
[21] L. Zhang, J. Gao, X. Chen, H. Tang, Y. Chen, Y. He, and Z. Yang, "A rapid vibration reduction method for macro–micro composite precision positioning stage," *IEEE Trans. Ind. Electron.*, vol. 64, no. 1, pp. 401–411, Jan. 2017.

CAOFENG YU received the B.S. degree in mechanical engineering and the Ph.D. degree in mine electromechanical engineering from the Anhui University of Science and Technology, Huainan, China, in 2011 and 2017, respectively.

He is currently an Associate Professor and a Master Tutor with the School of Mechanical Engineering, Anhui University of Science and Technology. His research interests include the development of giant magnetostrictive material devices and research on precision drive and control technology.

GAN WU received the B.S. degree from the Anhui University of Science and Technology, Huainan, in 2021, where he is currently pursuing the master's degree in electronic information instrument engineering. His research interests include driving mechanism and control technology of macro/micro actuator.

YU WANG received the B.S. degree from the Anhui University of Science and Technology, Huainan, China, in 2020, where she is currently pursuing the M.S. degree in mechanical engineering. Her research interests include driving mechanism and control technology of macro/micro actuator.

ZHIHAO XIAO received the B.S. degree from the Anhui University of Science and Technology, Huainan, China, in 2021, where he is currently pursuing the M.S. degree in mechanical engineering. His research interest includes high pressure common rail injector based on magnetostrictive effect of giant magnetostrictive material.

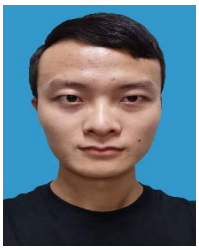

YONGYONG DUAN received the B.S. degree from the Anhui University of Science and Technology, Huainan, China, in 2021, where he is currently pursuing the M.S. degree in mechanical engineering. His research interest includes high pressure common rail injector based on magnetostrictive effect of giant magnetostrictive material.

ZHUO CHEN received the B.S. degree from the Henan College of Engineering, Henan, China, in 2020. He is currently pursuing the M.S. degree in mechanical engineering with the Anhui University of Science and Technology, Huainan, China. His research interest includes high pressure common rail injector based on magnetostrictive effect of giant magnetostrictive material.